Supporting Information

Tailored dealloying-driven, graphene-boosted defective rutile TiO_{2-x} for long-term lithium storage

Yang Chen [a], *Zhangfeng Li* [b], *Chaofan Yang* [a], *Dong Qiu* [a], *Chengli He* [a], *Zhiyu Jiang* [c], *Xiaoli Cui* [*, a]

[a] Department of Materials Science, Fudan University, Shanghai 200433, P. R. China

[b] Shanghai Institute of Space Power Sources, Shanghai 200245, P. R. China

[c] Department of Chemistry, Fudan University, Shanghai 200433, P. R. China

[*] Corresponding author, E-mail: xiaolicui@fudan.edu.cn

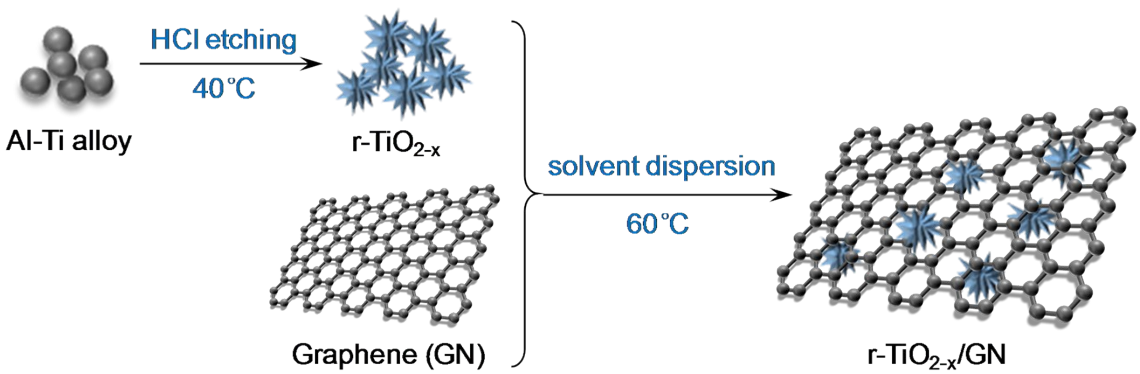

Figure S1 Schematic illustration of the synthesis of defective rutile TiO_2 (r-TiO_{2-x}) and r-TiO_{2-x}/graphene (r-TiO_{2-x}/GN) composites.

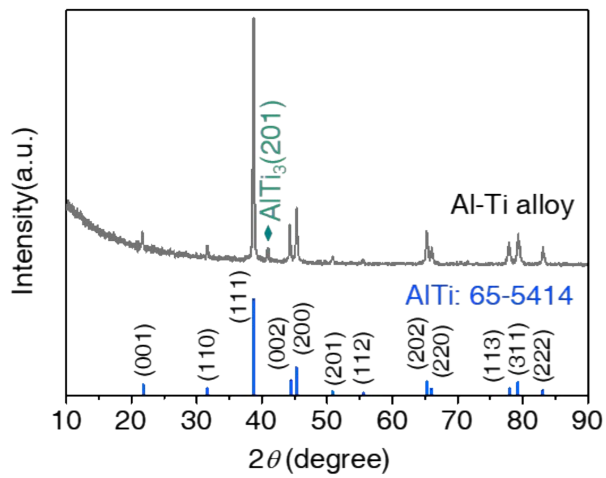

Figure S2 XRD pattern of Al-Ti alloy raw materials.

Note: The main diffraction peaks of the Al-Ti alloy precursors were assigned to tetragonal AlTi alloy referring to JCPDS card No: 65-5414, adopting the P4/mmm space group. A minor peak emerged at $2\theta = 40.9°$ was indexed to hexagonal $AlTi_3$ alloy (JCPDS No: 52-0859), P63/mmc space group. The little $AlTi_3$ alloy in final Al-Ti alloy products was inevitably introduced in the fabrication process due to a higher diffusion coefficient of Al than that of Ti. The main diffraction peak ($2\theta = 38.7°$) of AlTi alloy corresponded to (111) lattice plane, while the peak at $2\theta = 40.9°$ of $AlTi_3$ alloy was corresponding to (201) lattice plane. The intensity of main peaks was 13:1, thus, the content of AlTi alloy was estimated to be 93%.

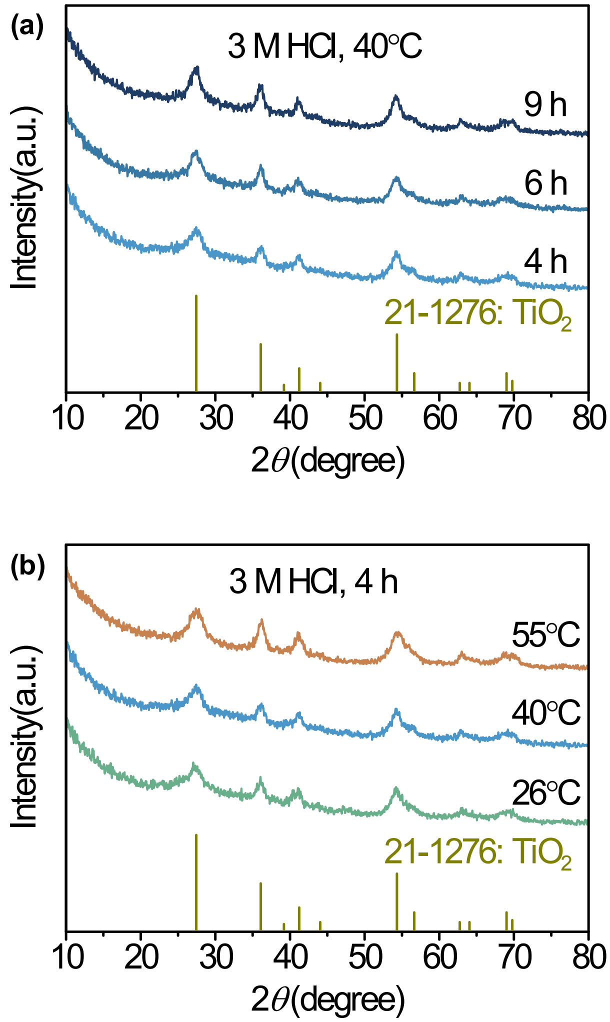

Figure S3 XRD patterns at different reaction times (a) and temperatures (b). All samples were obtained after centrifuging–rinsing–drying prior to characterizations.

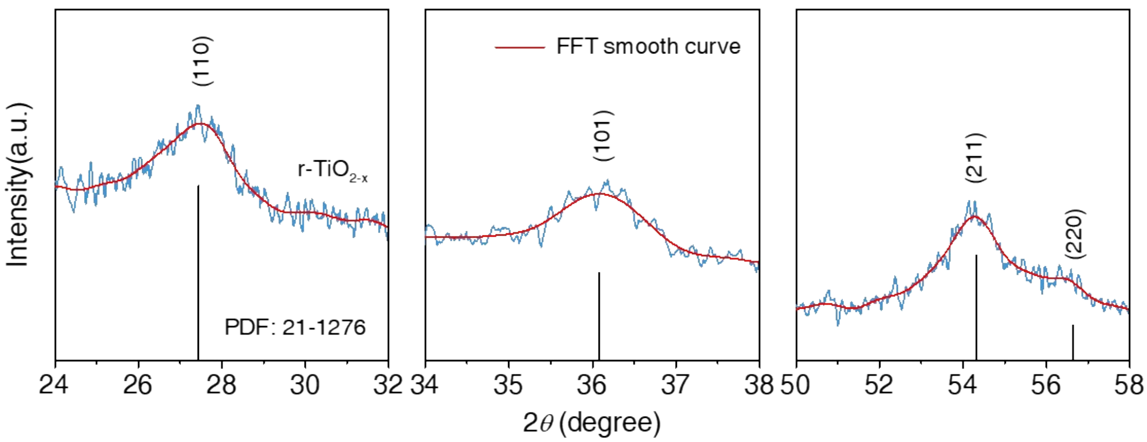

Figure S4 Partial enlarged XRD pattern of defective rutile TiO_{2-x} sample.

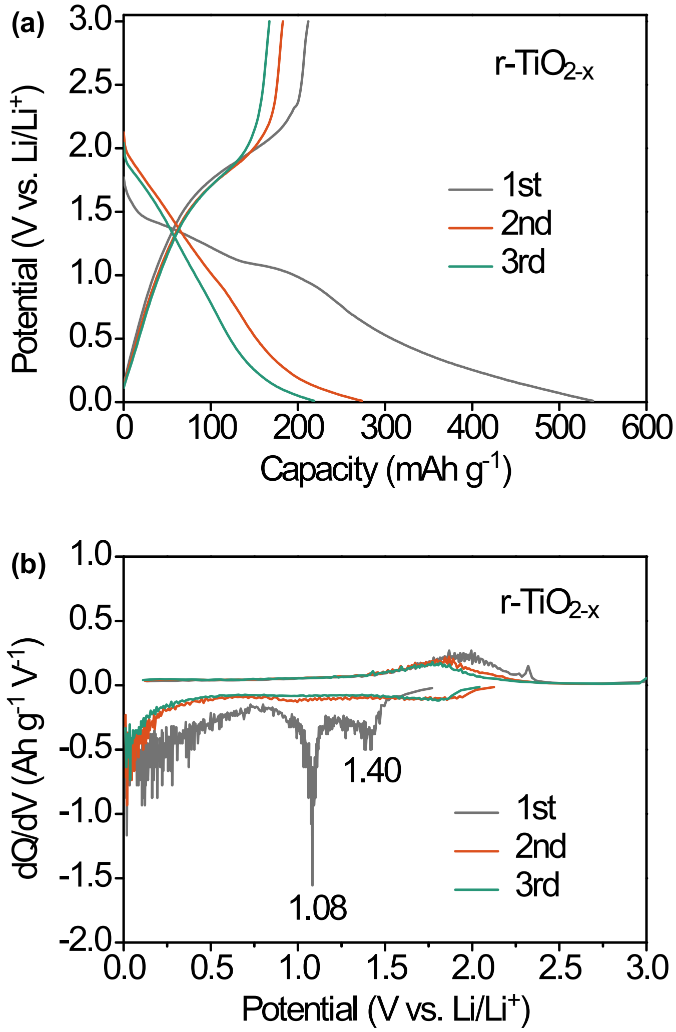

Figure S5 (a) First three-cycle voltage profiles of defective rutile TiO_{2-x} sample at 0.5C and (b) corresponding dQ/dV–potential plots.

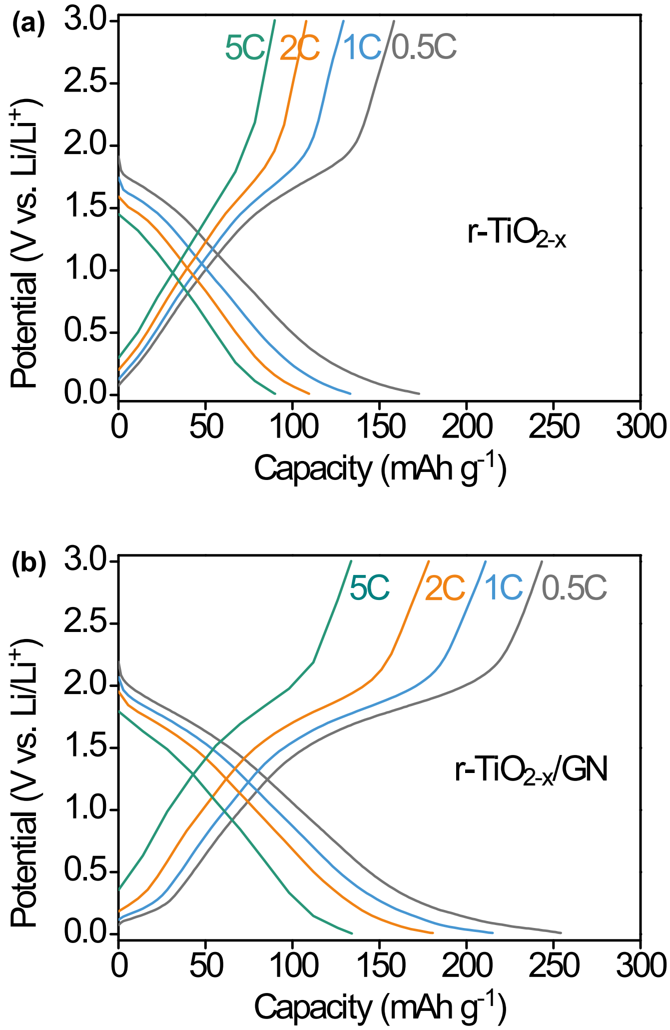

Figure S6 Voltage profiles of (a) r-TiO_{2-x} and (b) r-TiO_{2-x}/GN samples in a potential window of 0.01–3.0 V (vs. Li/Li^+).

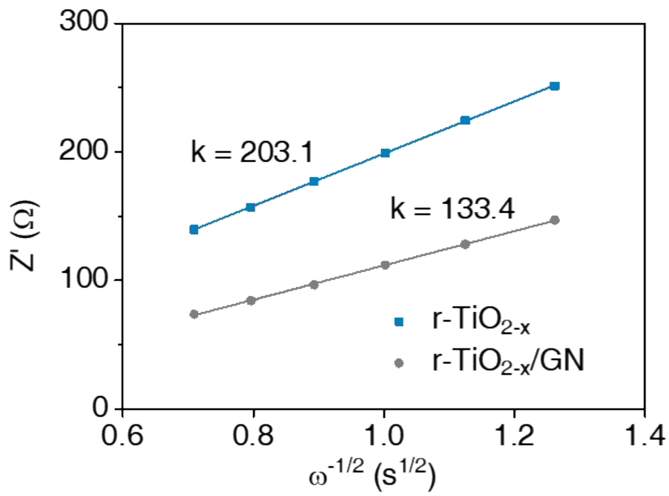

Figure S7 The relationship between Z’ and $\omega^{-1/2}$ taken from Nyquist plots.

Note: The low-frequency region in Nyquist plots (Figure 4f) is an inclined line, where the real part of impedance, Z', is proportional to $\omega^{-1/2}$ according to Equation S1 [1]. Thus, the Warburg factors (σ_w) of r-TiO_{2-x} and r-TiO_{2-x}/GN samples are fitted to be 203.1 and 133.4 $\Omega\ s^{-1/2}$, respectively.

$$Z^{'} = R_s + R_{ct} + \sigma_w \omega^{-1/2} \tag{S1}$$

Table S1 The grain sizes of r-TiO_{2-x} obtained after different etching time.

Etching time (h)	FWHM* (°)	Grain size (nm)
4 h	0.867	22.7
6 h	0.838	23.5
9 h	0.724	27.2

* Full width at half maximum (FWHM) of (110) lattice plane at $2\theta = 27.4°$.

Table S2 The electrochemical performance of rutile TiO_2 anode in lithium-ion batteries.

Electrode Materials	Potential window (V vs. Li/Li^+)	Reversible capacities (mAh g^{-1}/ mA g^{-1})	Initial C.E. (%)	Rate capability (mAh g^{-1}/ mA g^{-1})	Long-term cyclability (mAh g^{-1}/ mA g^{-1}/ cycles)	R_{ct} (Ω)	Ref./ Year
1 Rutile TiO_2							
Lotus-root shaped TiO_2	1.0-3.0	36/0.5C[(a)]	/	13/2C[(a)]	/	54[(b)]	[2]/2020
Nanoporous TiO_2 spheres	1.0-3.0	175[(b)]/67	/	75/3350	129/335/1000	149.7	[3]/2020
TiO_2 nanorods	1.0-3.0	143/170	84.3	76/1700	99/340/800	134.2	[4]/2019
TiO_2	1.0-4.5	200/34	72.7[(b)]	/	/	/	[5]/2019
Mesoporous TiO_2	1.0-3.0	220[(b)]/ 0.2C[(a)]	59.8[(b)]	70[(b)]/5C[(a)]	164/1C[(a)]/500	280	[6]/2019
Hierarchical TiO_2 microspheres	1.0-3.0	180[(b)]/84	62.5[(b)]	103/840	158/168/200	39.1	[7]/2018
Mesoporous TiO_2	1.0-3.0	243/170	86.0	78/8500	80/3400/2000	23.1[(c)]	[8]/2017
TiO_2 inverse opals	1.0-3.0	168/75	38.7[(b)]	137/450	95/450/5000	/	[9]/2017
TiO_2 nanoparticles	1.0-3.0	145/168	87.2	102/1675	143/168/80	/	[10]/2016
Hierarchical TiO_2	1.0-3.0	212/100	68.0[(b)]	100/2000	220/100/100	/	[11]/2016
Hierarchical TiO_2	0.01-3.0	350/100	66.0[(b)]	150/2000	346/100/100	/	[11]/2016
Hierarchical TiO_2	0.01-3.0	166/100	46.4	85/1675	190/100/200	100[(b)]	[12]/2016
Hierarchical mesoporous TiO_2 spheres	1.0-3.0	186/85	61.0	125/1700	/	44.3	[13]/2016
TiO_2 nanorod arrays	1.0-2.6	150[(d)]/5[(e)]	38.9	70[(d)]/200[(e)]	100[(d)]/100[(e)]/ 100	/	[14]/2016
Dandelion-like TiO_2	1.0-2.5	269/68	79.8	116/6800	/	70	[15]/2015
TiO_2 submicroboxes	1.0-3.0	238/170	44.0	68/5100	140[(b)]/850/500	/	[16]/2015
2 Rutile TiO_2/C composites							
TiO_2/C nanosheet	1.0-3.0	200/16.8	61.4	43/5040	110/840/2000	168	[17]/2019

Carbon/TiO_2 spheres	0.01-3.0	251/200	/	200/1000	219/500/200	50[b]	[18]/2016
TiO_2 mesocrystals/ reduced graphene oxide	1.0-3.0	215/168	72.4	140/6720	150/3360/1000	/	[19]/2015
TiO_2 nanoneedle/ graphene	1.0-3.0	170[b]/168	83.0[b]	149/840	/	65[b]	[20]/2015
TiO_2 nanobundles/ reduced graphene oxides	0.01-3.0	175[b]/200	54.4	78/2000	200/200/500	43.1	[21]/2014
TiO_2/carbon nanofibers	1.0-3.0	/	/	80/4200	190/100/500	32[b]	[22]/2014
3 Heteroatom-doped rutile TiO_2							
Sn-doped TiO_2 hollow nanocrystals	0.01-3.0	251/100	56.6	156/5000	110/5000/500	64.1[c]	[23]/2018
Nb-doped TiO_2	1.0-3.0	167/50	56.1	76/1000	100/250/80	/	[24]/2018
Nb-doped TiO_2	0.05-3.0	380/50	54.0	234/1000	280/250/80	/	[24]/2018
Nb-doped TiO_2 mesocrystals	1.0-3.0	199/0.5C[a]	70.3[b]	96/40C[a]	142/5C[a]/600	27	[25]/2017
Nb-doped TiO_2	1.0-3.0	220/170	68.0	120/16750	176/335/1000	/	[26]/2016
B-doped TiO_2 submicrospheres	1.0-3.0	166/168	62.1[b]	72/3350	190/335/500	259.4	[27]/2014
4 Defective rutile TiO_2							
TiO_{2-x}	1.0-3.0	254/100	93.8	220/300	/	34.4	[28]/2019
TiO_{2-x}/graphene quantum dots	1.0-3.0	169/5C[a]	67.6	145/15C[a]	160/10C[a]/500	54.6	[29]/2018
Ti^{3+} self-doped TiO_2 nanorods	1.0-3.0	169/168	72.6	92/8400	92/8400/1000	48.4[c]	[30]/2015
Hydrogenated TiO_2 nanoparticles	1.0-3.0	180/16.8	82.6	129/1680	/	27.2	[31]/2014
Ti^{3+} self-doped TiO_2/graphyne	0.01-3.0	195/84	42.0	134/840	157/168/1400	11.6	This work

Notes: [a]Unclear definition of 1C specific current [b]Estimated according to the figures. [c]Unit: $\Omega\ cm^{-2}$. [d]Unit: $\mu Ah\ cm^{-2}$. [e]Unit: $\mu A\ cm^{-2}$. "/" stands for no data given.

References

[1] Lu, K.; Hu, Z.; Xiang, Z.; Ma, J.; Song, B.; Zhang, J.; Ma, H., Cation intercalation in manganese oxide nanosheets: effects on lithium and sodium storage. *Angew. Chem. Int. Ed.* **2016**, *55*, 10448-10452.

[2] Choi, S. I.; Jung, E.-J.; Park, M.; Shin, H.-S.; Huh, S.; Won, Y. S., Phase-dependent performance of lotus-root shaped TiO_2 anode for lithium-ion batteries (LIBs). *Appl. Surf. Sci.* **2020**, *508*, 145237.

[3] Ma, D.; Li, K.; Pan, J. H., Ultraviolet-induced interfacial crystallization of uniform nanoporous biphasic TiO_2 spheres for durable lithium-ion battery. *ACS Appl. Energy Mater.* **2020**, *3* (5), 4186-4192.

[4] Lee, T. Y.; Lee, C. Y.; Chiu, H. T., Vapor-solid reaction growth of rutile TiO_2 nanorods and nanowires for Li-ion-battery electrodes. *ACS Omega* **2019**, *4* (14), 16217-16225.

[5] Christensen, C. K.; Mamakhel, M. A. H.; Balakrishna, A. R.; Iversen, B. B.; Chiang, Y. M.; Ravnsbaek, D. B., Order-disorder transition in nano-rutile TiO_2 anodes: a high capacity low-volume change Li-ion battery material. *Nanoscale* **2019**, *11* (25), 12347-12357.

[6] Ambade, R. B.; Koh, K. H.; Ambade, S. B.; Eom, W.; Noh, S. H.; Koo, C. M.; Kim, S. H.; Han, T. H., Kinetically controlled low-temperature solution-processed mesoporous rutile TiO_2 for high performance lithium-ion batteries. *J. Ind. Eng. Chem.* **2019**, *80*, 667-676.

[7] Chen, L.; Yang, S., Hierarchical rutile TiO_2 microspheres assembled by nanorods with nanocavities and their lithium-ion storage properties. *J. Nanopart. Res.* **2018**, *20* (2), 32.

[8] Wang, D.; Shan, Z.; Na, R.; Huang, W.; Tian, J., Solvothermal synthesis of hedgehog-like mesoporous rutile TiO_2 with improved lithium storage properties. *J. Power Sources* **2017**, *337*, 11-17.

[9] McNulty, D.; Carroll, E.; O'Dwyer, C., Rutile TiO_2 inverse opal anodes for Li-ion batteries with long cycle life, high-rate capability, and high structural stability. *Adv. Energy Mater.* **2017**, *7* (12), 1602291.

[10] Huang, J.; Fang, F.; Huang, G.; Sun, H.; Zhu, J.; Yu, R., Engineering the surface of rutile TiO_2 nanoparticles with quantum pits towards excellent lithium storage. *RSC Adv.* **2016**, *6* (70), 66197-66203.

[11] Hong, Z.; Hong, J.; Xie, C.; Huang, Z.; Wei, M., Hierarchical rutile TiO_2 with mesocrystalline structure for Li-ion and Na-ion storage. *Electrochim. Acta* **2016**, *202*, 203-208.

[12] Gao, R.; Jiao, Z.; Wang, Y.; Xu, L.; Xia, S.; Zhang, H., Eco-friendly synthesis of rutile TiO_2 nanostructures with controlled morphology for efficient lithium-ion batteries. *Chem. Eng. J.* **2016**, *304*, 156-164.

[13] Wang, W. L.; Park, J.-Y.; Nguyen, V. H.; Jin, E. M.; Gu, H.-B., Hierarchical mesoporous rutile TiO_2/C composite nanospheres as lithium-ion battery anode materials. *Ceram. Int.* **2016**, *42* (1), 598-606.

[14] Liu, G.; Zhang, S.; Wu, X.; Lin, R., Fabrication of rutile TiO_2 nanorod arrays on a copper substrate for high-performance lithium-ion batteries. *RSC Adv.* **2016**, *6* (60), 55671-55675.

[15] Bai, Y.; Liu, Z.; Zhang, N.; Sun, K., One-pot synthesis of 3-D dandelion-like architectures constructed by rutile TiO_2 nanorods grown along [001] axis for high-rate lithium ion batteries. *RSC Adv.* **2015**, *5* (27), 21285-21289.

[16] Yu, X. Y.; Wu, H. B.; Yu, L.; Ma, F. X.; Lou, X. W., Rutile TiO_2 submicroboxes with superior lithium storage properties. *Angew. Chem. Int. Ed.* **2015**, *54* (13), 4001-4004.

[17] Guan, Z.; Wang, X.; Li, T.; Zhu, Q.; Jia, M.; Xu, B., Facile synthesis of rutile TiO_2/carbon nanosheet composite from MAX phase for lithium storage. *J. Mater. Sci. Technol.* **2019**, *35* (9), 1977-1981.

[18] Zeng, T.; Ji, P.; Hu, X.; Li, G., Nano-Sn doped carbon-coated rutile TiO_2 spheres as a high capacity anode for Li-ion battery. *RSC Adv.* **2016**, *6* (54), 48530-48536.

[19] Lan, T.; Qiu, H.; Xie, F.; Yang, J.; Wei, M., Rutile TiO_2 mesocrystals/reduced graphene oxide with high-rate and long-term performance for lithium-ion batteries. *Sci. Rep.* **2015**, *5*, 8498.

[20] Gan, Y.; Zhu, L.; Qin, H.; Xia, Y.; Xiao, H.; Xu, L.; Ruan, L.; Liang, C.; Tao, X.; Huang, H.; Zhang, W., Hybrid nanoarchitecture of rutile TiO_2 nanoneedle/graphene for advanced lithium-ion batteries. *Solid State Ionics* **2015**, *269*, 44-50.

[21] Zhen, M.; Guo, X.; Gao, G.; Zhou, Z.; Liu, L., Rutile TiO_2 nanobundles on reduced graphene oxides as anode materials for Li ion batteries. *Chem. Commun.* **2014**, *50* (80), 11915-11918.

[22] Kong, J.; Wei, Y.; Zhao, C.; Toh, M. Y.; Yee, W. A.; Zhou, D.; Phua, S. L.; Dong, Y.; Lu, X., Growth of rutile TiO_2 on the convex surface of nanocylinders: from

nanoneedles to nanorods and their electrochemical properties. *Nanoscale* **2014**, *6* (8), 4352-4360.

[23] Jiao, S.; Lian, G.; Jing, L.; Xu, Z.; Wang, Q.; Cui, D.; Wong, C.-P., Sn-doped rutile TiO_2 hollow nanocrystals with enhanced lithium-ion batteries performance. *ACS Omega* **2018**, *3* (1), 1329-1337.

[24] Gardecka, A. J.; Lübke, M.; Armer, C. F.; Ning, D.; Reddy, M. V.; Williams, A. S.; Lowe, A.; Liu, Z.; Parkin, I. P.; Darr, J. A., Nb-doped rutile titanium dioxide nanorods for lithium-ion batteries. *Solid State Sci.* **2018**, *83*, 115-121.

[25] Lan, T.; Zhang, W.; Wu, N. L.; Wei, M., Nb-doped rutile TiO_2 mesocrystals with enhanced lithium storage properties for lithium ion battery. *Chem. Eur. J.* **2017**, *23* (21), 5059-5065.

[26] Usui, H.; Domi, Y.; Yoshioka, S.; Kojima, K.; Sakaguchi, H., Electrochemical lithiation and sodiation of Nb-doped rutile TiO_2. *ACS Sustain. Chem. Eng.* **2016**, *4* (12), 6695-6702.

[27] Tian, H.; Xin, F.; Tan, X.; Han, W., High lithium electroactivity of boron-doped hierarchical rutile submicrosphere TiO_2. *J. Mater. Chem. A* **2014**, *2* (27), 10599-10606.

[28] Kang, S. H.; Jo, Y. N.; Prasanna, K.; Santhoshkumar, P.; Joe, Y. C.; Vediappan, K.; Gnanamuthu, R.; Lee, C. W., Bandgap tuned and oxygen vacant TiO_{2-x} anode materials with enhanced electrochemical properties for lithium ion batteries. *J. Ind. Eng. Chem.* **2019**, *71*, 177-183.

[29] Zhang, W.; Xu, T.; Liu, Z.; Wu, N. L.; Wei, M., Hierarchical TiO_{2-x} imbedded with graphene quantum dots for high-performance lithium storage. *Chem. Commun.* **2018**, *54* (12), 1413-1416.

[30] Chen, J.; Song, W.; Hou, H.; Zhang, Y.; Jing, M.; Jia, X.; Ji, X., Ti^{3+} self-doped dark rutile TiO_2 ultrafine nanorods with durable high-rate capability for lithium-ion batteries. *Adv. Funct. Mater.* **2015**, *25* (43), 6793-6801.

[31] Qiu, J.; Li, S.; Gray, E.; Liu, H.; Gu, Q.-F.; Sun, C.; Lai, C.; Zhao, H.; Zhang, S., Hydrogenation synthesis of blue TiO_2 for high-performance lithium-ion batteries. *J. Phys. Chem. C* **2014**, *118* (17), 8824-8830.